JHEP

Published for SISSA by Springer

Received: November 9, 2017
Accepted: March 3, 2018
Published: March 28, 2018

Combination of KLOE $\sigma\left(e^+e^- \to \pi^+\pi^-\gamma(\gamma)\right)$ measurements and determination of $a_\mu^{\pi^+\pi^-}$ in the energy range $0.10 < s < 0.95\,\mathrm{GeV}^2$

The KLOE-2 collaboration

A. Anastasi,[e,c] D. Babusci,[c] M. Berlowski,[c,v] C. Bloise,[c] F. Bossi,[c] P. Branchini,[s] A. Budano,[r,s] L. Caldeira Balkeståhl,[u] B. Cao,[u] F. Ceradini,[r,s] P. Ciambrone,[c] F. Curciarello,[c] E. Czerwiński,[b] G. D'Agostini,[n,o] E. Danè,[c] V. De Leo,[q] E. De Lucia,[c] A. De Santis,[c] P. De Simone,[c] A. Di Cicco,[r,s] A. Di Domenico,[n,o] D. Domenici,[c] A. D'Uffizi,[c] A. Fantini,[p,q] G. Fantini,[d] P. Fermani,[c] S. Fiore,[t,o] A. Gajos,[b] P. Gauzzi,[n,o] S. Giovannella,[c] E. Graziani,[s] V. L. Ivanov,[g,h] T. Johansson,[u] X. Kang,[c] D. Kisielewska-Kamińska,[b] E. A. Kozyrev,[g,h] W. Krzemien,[v] A. Kupsc,[u] S. Loffredo,[r,s] P. A. Lukin,[g,h] G. Mandaglio,[f,a] M. Martini,[c,m] R. Messi,[p,q] S. Miscetti,[c] G. Morello,[c] D. Moricciani,[q] P. Moskal,[b] A. Passeri,[s] V. Patera,[l,o] E. Perez del Rio,[c] N. Raha,[q] P. Santangelo,[c] M. Schioppa,[j,k] A. Selce,[r,s] M. Silarski,[b] F. Sirghi,[c] E. P. Solodov,[g,h] L. Tortora,[s] G. Venanzoni[i,1] W. Wiślicki[v] and M. Wolke,[u]

A. Keshavarzi[w,1] S.E. Müller[x] and T. Teubner[w]

[a] *INFN Sezione di Catania, Catania, Italy*
[b] *Institute of Physics, Jagiellonian University, Cracow, Poland*
[c] *Laboratori Nazionali di Frascati dell'INFN, Frascati, Italy*
[d] *Gran Sasso Science Institute, L'Aquila, Italy*
[e] *Dipartimento di Scienze Matematiche e Informatiche, Scienze Fisiche e Scienze della Terra, Università di Messina, Messina, Italy*
[f] *Dipartimento di Scienze Chimiche, Biologiche, Farmaceutiche ed Ambientali, Università di Messina, Messina, Italy*
[g] *Budker Institute of Nuclear Physics, Novosibirsk, Russia*
[h] *Novosibirsk State University, Novosibirsk, Russia*
[i] *INFN Sezione di Pisa, Pisa, Italy*
[j] *Dipartimento di Fisica, Università della Calabria, Rende, Italy*
[k] *INFN Gruppo collegato di Cosenza, Rende, Italy*
[l] *Dipartimento di Scienze di Base ed Applicate per l'Ingegneria, Università "Sapienza", Roma, Italy*

[1] Corresponding author.

https://doi.org/10.1007/JHEP03(2018)173

JHEP03(2018)173

[m] *Dipartimento di Scienze e Tecnologie applicate, Università "Guglielmo Marconi", Roma, Italy*
[n] *Dipartimento di Fisica, Università "Sapienza", Roma, Italy*
[o] *INFN Sezione di Roma, Roma, Italy*
[p] *Dipartimento di Fisica, Università "Tor Vergata", Roma, Italy*
[q] *INFN Sezione di Roma Tor Vergata, Roma, Italy*
[r] *Dipartimento di Matematica e Fisica, Università "Roma Tre", Roma, Italy*
[s] *INFN Sezione di Roma Tre, Roma, Italy*
[t] *ENEA, Department of Fusion and Technology for Nuclear Safety and Security, Frascati (RM), Italy*
[u] *Department of Physics and Astronomy, Uppsala University, Uppsala, Sweden*
[v] *National Centre for Nuclear Research, Warsaw, Poland*
[w] *Department of Mathematical Sciences, University of Liverpool, Liverpool L69 3BX, U.K.*
[x] *Department of Information Services and Computing & Institute of Radiation Physics, Helmholtz-Zentrum Dresden-Rossendorf, Dresden, Germany*

E-mail: graziano.venanzoni@lnf.infn.it, a.i.Keshavarzi@liverpool.ac.uk

Abstract: The three precision measurements of the cross section $\sigma\left(e^+e^- \to \pi^+\pi^-\gamma(\gamma)\right)$ using initial state radiation by the KLOE collaboration provide an important input for the prediction of the hadronic contribution to the anomalous magnetic moment of the muon. These measurements are correlated for both statistical and systematic uncertainties and, therefore, the simultaneous use of these measurements requires covariance matrices that fully describe the correlations. We present the construction of these covariance matrices and use them to determine a combined KLOE measurement for $\sigma\left(e^+e^- \to \pi^+\pi^-\gamma(\gamma)\right)$. We find, from this combination, a two-pion contribution to the muon magnetic anomaly in the energy range $0.10 < s < 0.95\,\mathrm{GeV}^2$ of $a_\mu^{\pi^+\pi^-} = (489.8 \pm 1.7_{\mathrm{stat}} \pm 4.8_{\mathrm{sys}}) \times 10^{-10}$.

Data vectors and covariance matrices are available at http://www.lnf.infn.it/kloe/ppg/ppg_2017/ppg_2017.html.

Keywords: e+-e- Experiments

ArXiv ePrint: 1711.03085

JHEP03(2018)173

Contents

JHEP03(2018)173

1 Introduction

The KLOE collaboration have made three precise measurements of the cross section $\sigma(e^+e^- \to \pi^+\pi^-\gamma(\gamma))$ in 2008 [1, 2], 2010 [3, 4] and 2012 [5, 6].[1] These measurements are crucial for estimating the hadronic vacuum polarisation (HVP) contribution to the anomalous magnetic moment of the muon, $a_\mu^{\rm HVP}$, which is presently the limiting factor in the precision of the Standard Model (SM) prediction, $a_\mu^{\rm SM}$. This SM prediction disagrees with the experimental value, $a_\mu^{\rm exp}$ [8–11], by approximately 3.5 standard deviations or higher [12–19], making it an interesting probe of potential physics beyond the SM. Currently, the uncertainties of $a_\mu^{\rm SM}$ and $a_\mu^{\rm exp}$ are of comparable magnitude. However, with new experimental efforts at Fermilab [20] and J-PARC [21] set to improve the experimental error by a factor of four compared to the BNL measurements [8–10], it is imperative that the SM prediction is also improved.

The HVP contribution to $a_\mu^{\rm SM}$ can be determined using a dispersion integral and the cross section $\sigma^0(e^+e^- \to \text{hadrons})$, which is bare (undressed of all vacuum polarisation

[1] The KLOE collaboration also made a measurement of $\sigma(e^+e^- \to \pi^+\pi^-\gamma(\gamma))$ in 2005 [7]. However, this is now considered to be superseded by the 2008 measurement, as discussed in [1].

(VP) effects) as indicated by the superscript '0', but includes final state radiation (FSR). At leading order (LO), the dispersion integral is

$$a_\mu^{\mathrm{LO,HVP}} = \frac{1}{4\pi^3}\int_{s_{th}}^{\infty} \mathrm{d}s\ \sigma^0_{\mathrm{had}}(s)K(s)\,, \tag{1.1}$$

where $s_{th} = m^2_{\pi^0}$ is the hadronic production threshold, $\sigma^0_{\mathrm{had}}(s)$ is the bare cross section of the process $e^+e^- \to$ hadrons and $K(s)$ is a well-known kernel function [22, 23]. The contribution of the $\pi^+\pi^-$ final state to the anomalous magnetic moment of the muon, $a_\mu^{\pi^+\pi^-}$, is over 70% of the total estimate of a_μ^{HVP} and is also the largest contributor to its uncertainty. Consequently, the three measurements of the cross section $\sigma^0\big(e^+e^- \to \pi^+\pi^-\gamma(\gamma)\big)$ by the KLOE collaboration are invaluable to precisely determine $a_\mu^{\pi^+\pi^-}$.

The simultaneous input of the KLOE measurements into equation (1.1) requires a detailed analysis to attain the correct combination of the three, which will have a non-trivial influence on $a_\mu^{\pi^+\pi^-}$ and provide an important comparison with other experimental measurements of $\sigma_{\pi\pi}$. The KLOE measurements of $\sigma_{\pi\pi(\gamma)}$ are, in part, highly correlated, necessitating the construction of full statistical and systematic covariance matrices to be used in any combination of these data. To combine the data without the correlations would result in an underestimate of the uncertainty of a_μ^{HVP} and, potentially, a bias of its mean value. The construction of these covariance matrices must be statistically robust in order to ensure that they correctly describe the correlated relationship of the three measurements.

The main purpose of this work is to formulate the covariance matrices required to determine the correct combination. In section 2, the three KLOE measurements of $\sigma\big(e^+e^- \to \pi^+\pi^-\gamma(\gamma)\big)$ [1–6] are reviewed and, in some cases, updated in order to ensure a consistent combination. Section 3 then focuses on the construction of the statistical and systematic covariance matrices for the combination of the KLOE measurements. In section 4, these matrices are then used to combine the three measurements into a single measurement of $\sigma^0\big(e^+e^- \to \pi^+\pi^-\gamma(\gamma)\big)$, which we use to provide an estimate of $a_\mu^{\pi^+\pi^-}$. We then compare our results with the individual KLOE measurements and other experimental measurements of $\sigma_{\pi\pi(\gamma)}$.

2 Measurements of $\sigma^0\big(e^+e^- \to \pi^+\pi^-\gamma(\gamma)\big)$ by the KLOE collaboration

2.1 Determination of the $\pi^+\pi^-$ cross section

DAΦNE [24] is a high luminosity e^+e^- collider that operates predominantly at the centre of mass energy equal to the ϕ meson mass, $\sqrt{s} = m_\phi = 1.0194$ GeV [11]. The KLOE detector has been used to obtain measurements of the process $e^+e^- \to \pi^+\pi^-\gamma(\gamma)$ [1, 3, 5, 25, 26]. These measurements are achieved through radiative return, where the differential cross section is measured as a function of the invariant mass of the pion pair, $\sqrt{s'} = M_{\pi\pi}$. The cross section $\sigma_{\pi\pi} \equiv \sigma(e^+e^- \to \pi^+\pi^-)$ is then determined according to [27–30] using the relation

$$s\frac{\mathrm{d}\sigma\big(\pi^+\pi^-\gamma\big)}{dM^2_{\pi\pi}} = \sigma_{\pi\pi}(M^2_{\pi\pi})H(M^2_{\pi\pi}, s)\,, \tag{2.1}$$

JHEP03(2018)173

where H is the radiator function describing the emission of photons in the initial state [31–34]. Equation (2.1) is valid neglecting the contribution from FSR, although it is properly accounted for in the KLOE analyses [1, 3, 5, 35].

The KLOE collaboration have performed three measurements of the cross section $\sigma\big(e^+e^- \to \pi^+\pi^-\gamma(\gamma)\big)$ [1–6]. All three published cross sections are bare (undressed of all VP effects) and including FSR. For the first two, which for the purposes of this study we shall denote as KLOE08 [1] and KLOE10 [3], the bare cross section is obtained by [36, 37]

$$\sigma^0_{\pi\pi(\gamma)}(s') = \sigma_{\pi\pi(\gamma)}(s')|1 - \Pi(s')|^2, \tag{2.2}$$

where the superscript '0' indicates that the cross section is bare, the subscript (γ) indicates that the cross section includes FSR, $\sigma_{\pi\pi(\gamma)}(s')$ is obtained using equation (2.1) and $\Pi(s')$ is the vacuum polarisation containing both real and imaginary parts [38].[2]

For the third measurement of $\sigma^0_{\pi\pi(\gamma)}(s')$, namely KLOE12 [5], a reciprocal relation to equation (2.1) was utilised, allowing for a bin-by-bin normalisation of the $\pi^+\pi^-$ cross section by the $\mu^+\mu^-$ cross section. For the same invariant mass squared, the ratio of the $\pi^+\pi^-\gamma$ and $\mu^+\mu^-\gamma$ differential cross sections allows the relation

$$\sigma^0_{\pi\pi(\gamma)}(s') = \frac{\mathrm{d}\sigma\big(\pi^+\pi^-\gamma\big)/\mathrm{d}s'}{\mathrm{d}\sigma\big(\mu^+\mu^-\gamma\big)/\mathrm{d}s'} \times \sigma^0_{(\gamma)}(e^+e^- \to \mu^+\mu^-, s')\,, \tag{2.3}$$

where $s' = M^2_{\pi\pi} = M^2_{\mu\mu}$. This normalisation has many advantages concerning the determination of the cross section. Importantly, the ratio in equation (2.3) benefits from the cancellation of the radiator function for initial state radiation (ISR) and of the VP correction, manifestly resulting in a bare cross section. Therefore, the undressing procedure described by equation (2.2) is not applied to KLOE12, although the FSR contribution to the $\pi^+\pi^-$ production must again be included.

The pion form factor, $|F_\pi|^2$, is determined for all three measurements to be

$$\big|F_\pi(s')\big|^2 = \frac{3}{\pi}\frac{s'}{\alpha^2\beta^3_\pi(s')}\frac{\sigma^0_{\pi\pi(\gamma)}(s')}{|1-\Pi(s')|^2}\Big(1 - \frac{\alpha}{\pi}\eta_\pi(s')\Big)\,, \tag{2.4}$$

where $\alpha \equiv \alpha(0)$, $\beta_\pi(s') = \sqrt{1 - 4m^2_\pi/s'}$ and η_π is the inclusive FSR correction assuming point-like pions [39].

2.2 The KLOE measurements

The experimental analysis of each KLOE measurement of $\sigma\big(e^+e^- \to \pi^+\pi^-\gamma(\gamma)\big)$ has been reviewed and, in some cases, updated in order to ensure a more precise and consistent combination of the three measurements. In the following, each measurement is discussed individually, where any changes to the respective analysis are explicitly stated.

[2]The correction used previously for KLOE08 [1, 2] and KLOE10 [3, 4] contained only the real part of the VP. This has been updated in this analysis to incorporate the full VP with both the real and imaginary parts, where the imaginary part is small and sub-leading compared to the real contribution (see section 2.2 for more details).

JHEP03(2018)173

The KLOE08 measurement consists of 60 data points in the range $0.35 < s' < 0.95\,\mathrm{GeV}^2$, covering the dominant ρ resonance structure and the $\rho - \omega$ interference region in the $\pi^+\pi^-$ final state. The uncertainties of the cross section are dominated by the systematics uncertainties, especially in the region where the cross section is large. The KLOE08 data have been updated with respect to [1] to incorporate the following necessary changes:

- The data have been undressed of VP effects using an updated routine [36, 37] compared to the one used previously [40], which now corrects the data using a more appropriate energy grid parametrisation for the determination of the VP.
- The VP correction contains both real and imaginary parts, whereas previously the data were only corrected for the real part of the VP.
- The data are not rounded as they were in [1] to ensure that the statistical and systematic uncertainties correspond to the variances that enter into the diagonal elements of the corresponding covariance matrices.
- The calculation of the cross section has been updated with respect to the precision of input parameters and fundamental constants [11].

We find, using the updated data for KLOE08, a contribution to the anomalous magnetic moment of the muon of

$$a_\mu^{\pi^+\pi^-}(\mathrm{KLOE08}, 0.35 < s' < 0.95\ \mathrm{GeV}^2) = (386.6 \pm 0.4_{\mathrm{stat}} \pm 3.3_{\mathrm{sys}}) \times 10^{-10}, \qquad (2.5)$$

which exhibits a decrease in the mean value of $a_\mu^{\pi^+\pi^-}$ when compared to the estimate quoted in [1] that is largely due to the updated determination of the VP. The updated cross section and pion form factor vectors with corresponding covariance matrices for the statistical and systematic uncertainties are available from [41].

The KLOE10 measurement totals 75 data points in the range $0.1 < s' < 0.85\,\mathrm{GeV}^2$. This analysis [3] selected events that included a photon detected in the calorimeter at large polar angle, allowing the measurement to be taken at lower s' closer to threshold. The fifty energy bins of the data in the range $0.35 < s' < 0.85\,\mathrm{GeV}^2$ are identical to the fifty KLOE08 bins in the same interval. The KLOE10 cross section has been updated in the same way as KLOE08, with the application of the improved VP correction [36, 37], the non-rounded data and improved parameter precision resulting in

$$a_\mu^{\pi^+\pi^-}(\mathrm{KLOE10}, 0.10 < s' < 0.85\ \mathrm{GeV}^2) = (477.9 \pm 2.0_{\mathrm{stat}} \pm 6.7_{\mathrm{sys}}) \times 10^{-10}, \qquad (2.6)$$

which, like observed with KLOE08, results in a decrease in the mean value of $a_\mu^{\pi^+\pi^-}$ compared to the estimate in [3]. The updated KLOE10 data vectors and covariance matrices are available from [41].

The KLOE12 measurement was determined as a $\mu^+\mu^-\gamma$ normalised cross section, as described briefly in section 2.1. The $\mu^+\mu^-$ cross section was measured for the analysis, whereas the KLOE08 $\pi^+\pi^-$ data were used as the input into equation (2.3), with the KLOE12 measurement having an identical binning and energy range to KLOE08. As these

JHEP03(2018)173

measurements share the same two-pion data, KLOE08 and KLOE12 are highly correlated and it is imperative that they be treated as such in any combination of the two measurements. The KLOE12 cross section has been updated with respect to the use of non-rounded data and input parameter precision. The ratio in equation (2.3) benefits from the cancellation of the VP correction and, therefore, does not require an updated VP correction as with the KLOE08 and KLOE10 cross section data. For the contribution to the muon magnetic anomaly, from the KLOE12 data alone, we find

$$a_\mu^{\pi^+\pi^-}(\text{KLOE12}, 0.35 < s' < 0.95\ \text{GeV}^2) = (385.1 \pm 1.2_{\text{stat}} \pm 2.3_{\text{sys}}) \times 10^{-10}. \tag{2.7}$$

Here, the error has reduced since [5], where a flaw in the previous error calculation resulted in an overestimation of the published systematic uncertainty and, as a result, there have been necessary changes to the KLOE12 systematic matrix construction.[3] The updated KLOE12 data are available from [41].

3 Constructing the KLOE combination covariance matrices

The flow of the experimental analyses for the KLOE08, KLOE10 and KLOE12 measurements is shown in figure 1. In the case of the KLOE12 measurement, the beginning of the flow refers to the measurement of $\mu^+\mu^-\gamma(\gamma)$. The point where the KLOE08 $\pi^+\pi^-\gamma(\gamma)$ data enters is clearly marked. This diagram exhibits the extent of the correlation between KLOE08 and KLOE12, with correlations existing for all elements of the KLOE08 $\sigma_{\pi\pi}$ analysis from the observed spectrum of $\pi^+\pi^-\gamma(\gamma)$ events up to the acceptance correction. In addition, the degree of correlation between KLOE08 and KLOE10 or KLOE10 and KLOE12 is clearly shown, with many parts of the experimental analyses being common to a pair of measurements or having been obtained through a similar method.

The KLOE statistical and systematic combination covariance matrices are 195×195 matrices and are depicted in figure 2. They have been carefully constructed to satisfy the necessary mathematical properties of a covariance matrix, details of which are described in appendix A. The KLOE08, KLOE10 and KLOE12 diagonal blocks are simply the covariance matrices of the individual measurements. The KLOE0810 block describes the correlation between KLOE08 and KLOE10, with corresponding definitions for KLOE0812 and KLOE1012. Statistical uncertainties are, in general, uncorrelated ($\rho_{ij}^{\alpha_{\text{stat}}}|_{i\neq j} = 0$, where ρ_{ij} is the correlation coefficient defined in appendix A) and only contribute to the diagonal elements of the corresponding correlation block of the combination covariance matrix. The exceptions to this are the unfolding and unshifting corrections[4] (see section 3.1), which both contribute to the non-diagonal elements of the statistical matrix ($\rho_{ij}^{\alpha_{\text{stat}}} = -1 \leq \rho \leq 1$). For systematic (sys) uncertainties, all data points are taken to be 100% correlated or anti-correlated ($\rho_{ij}^{\alpha_{\text{sys}}} = \pm 1$). The resulting correlation structures for both the statistical and

[3] The KLOE12 systematic uncertainty has reduced from 2.7×10^{-10} given in [5] to 2.3×10^{-10} in this analysis.

[4] While the unfolding correction accounts for the smearing due to the detector resolution, the unshifting is a redistribution correction that accounts for photons emitted through final state radiation, which results in shifting the observed value of s' away from the squared invariant mass of the virtual photon s_γ^* [35].

JHEP03(2018)173

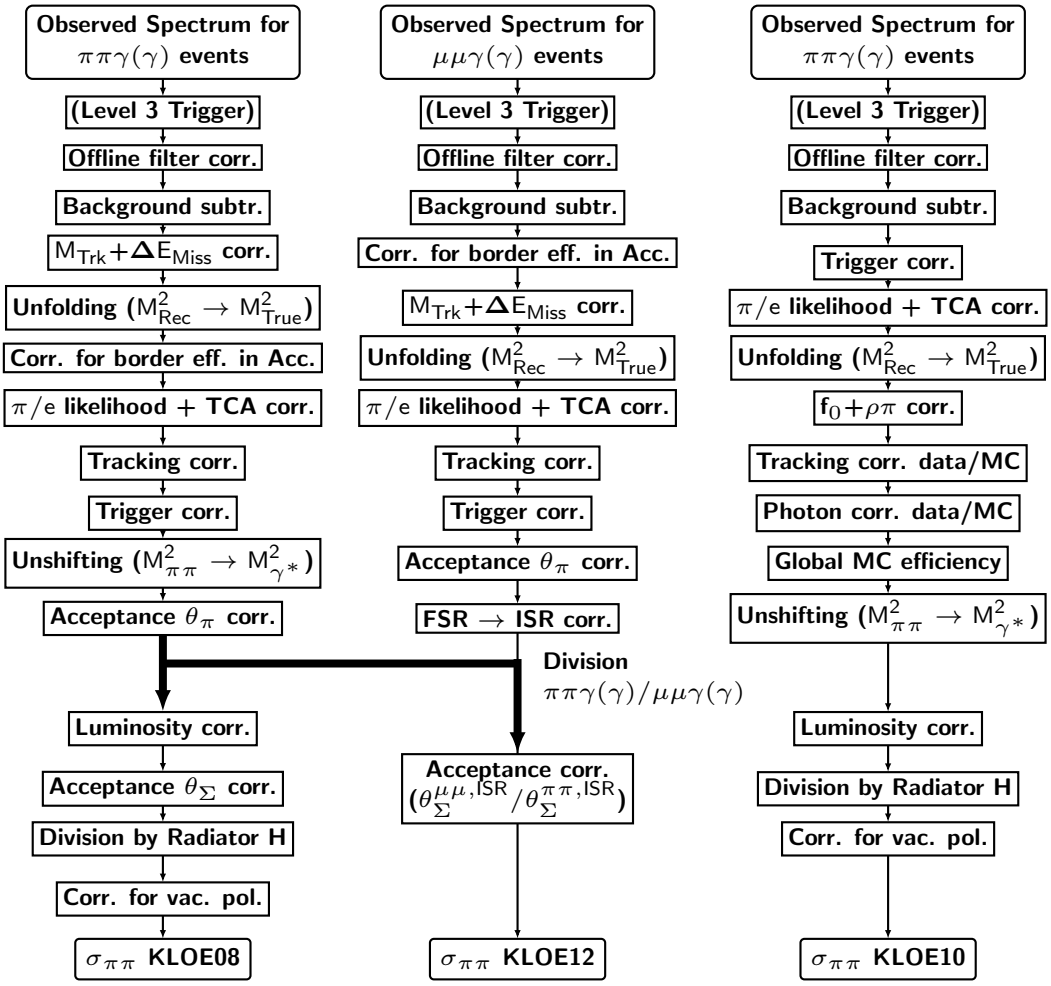

Figure 1. The flow of the experimental analyses of all three $\sigma^0\big(e^+e^- \to \pi^+\pi^-\gamma(\gamma)\big)$ cross section measurements. The point where the KLOE08 $\pi^+\pi^-\gamma(\gamma)$ data enter the KLOE12 analysis is indicated by the bold black arrows.

systematic matrix are shown in figure 3. In the following, we outline the correlations that exist for and between the individual measurements for the statistical and systematic uncertainties separately.

3.1 Statistical correlations

Other than those that exist as part of the individual analyses for the KLOE08, KLOE10 and KLOE12 diagonal sub-matrices in the statistical 195 × 195 combination covariance matrix depicted in figure 2, the only statistical correlations that are present are those due to the two-pion data that are shared between KLOE08 and KLOE12. These occupy the KLOE0812 and KLOE1208 blocks of the statistical combination covariance matrix. As no statistical correlations exist between KLOE08 and KLOE10 or KLOE10 and KLOE12, all elements of the KLOE0810 (KLOE1008) and KLOE1012 (KLOE1210) correlation blocks of the statistical covariance matrix are zero. This can be seen diagrammatically in figure 3.

JHEP03(2018)173

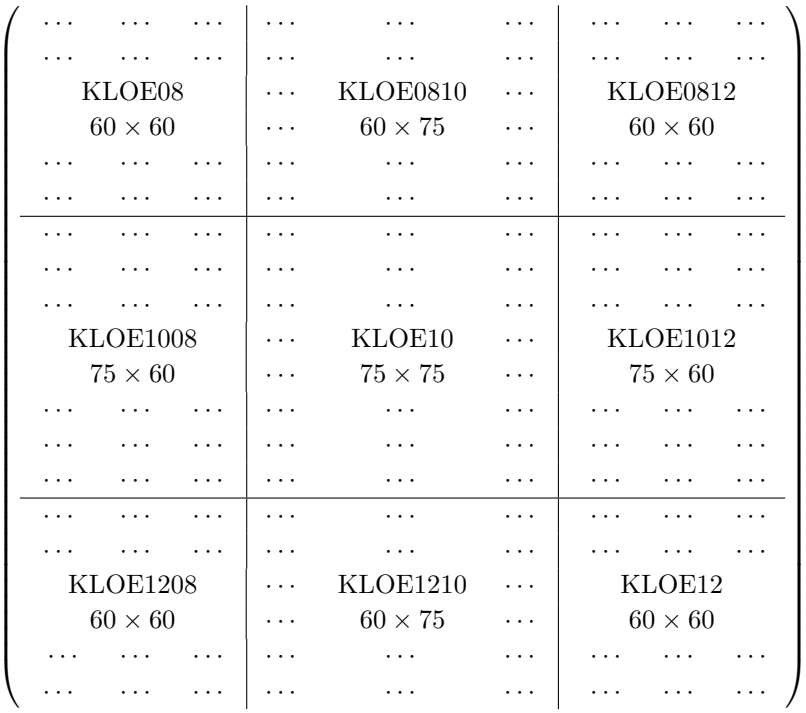

Figure 2. The KLOE $\pi^+\pi^-\gamma(\gamma)$ combination matrix structure for both the statistical and systematic covariance matrices.

The individual KLOE08, KLOE10 and KLOE12 statistical covariance matrices (corresponding to the diagonal blocks of the statistical combination matrix given by figure 2) describe all statistical uncertainties inherent in the respective experimental analysis. The contributions to the statistical covariance matrices from the unfolding and unshifting procedures are partially correlated, where the correlation coefficients are defined by the unfolding [42–44] and unshifting [42] procedures themselves. Details regarding these procedures and all other statistical uncertainties (which are considered to be fully uncorrelated) can be found in [2, 4, 6].

The KLOE0812 statistical correlation block receives contributions from all corrections to the KLOE08 $\pi^+\pi^-\gamma(\gamma)$ data up until the point where these data enter the KLOE12 analysis. Following the experimental analysis flow for KLOE08 in figure 1, these include the detector resolution correction (unfolding), the correction for border efficiency in the acceptance, the pion identification efficiency (π/ε likelihood), the tracking efficiency, the trigger corrections, the unshifting of $M^2_{\pi\pi} \to (M^0_{\pi\pi})^2$ and the acceptance for the cuts in θ_π and $\theta_{\pi\pi}$ [2]. All corrections prior to the unfolding in the analysis flow are included in the unfolded KLOE08 $\pi^+\pi^-\gamma(\gamma)$ spectrum and, therefore, manifestly enter the KLOE0812 correlations through the correlations of the unfolding. As the unfolding (unf) and unshifting (uns) corrections are identically correlated for the KLOE08 and KLOE12 statistical covariance matrices, these correlations must be reflected in the KLOE0812 correlation block exactly in the form

$$\rho_{ij}^{0812,\mathrm{unf/uns}} = \rho_{ji}^{1208,\mathrm{unf/uns}} = \rho_{ij}^{08,\mathrm{unf/uns}} = \rho_{ij}^{12,\mathrm{unf/uns}}. \tag{3.1}$$

JHEP03(2018)173

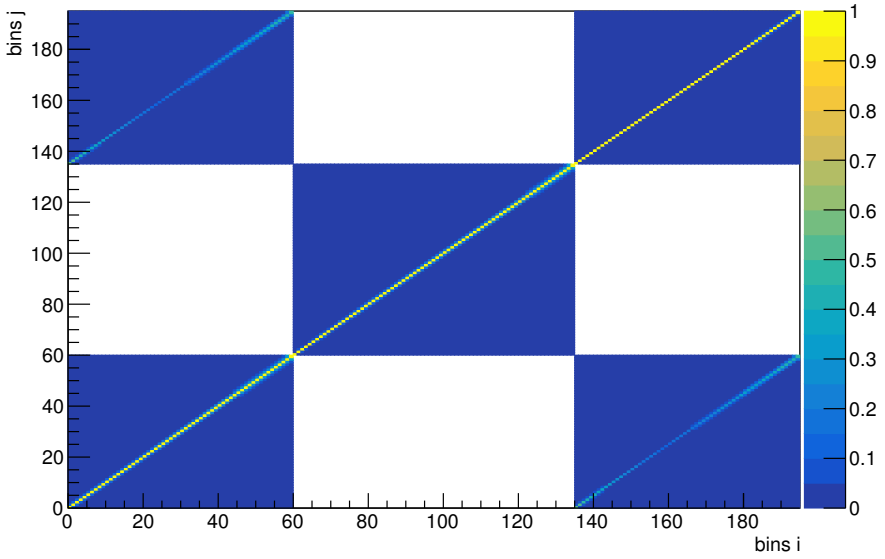

(a) Statistical correlation matrix

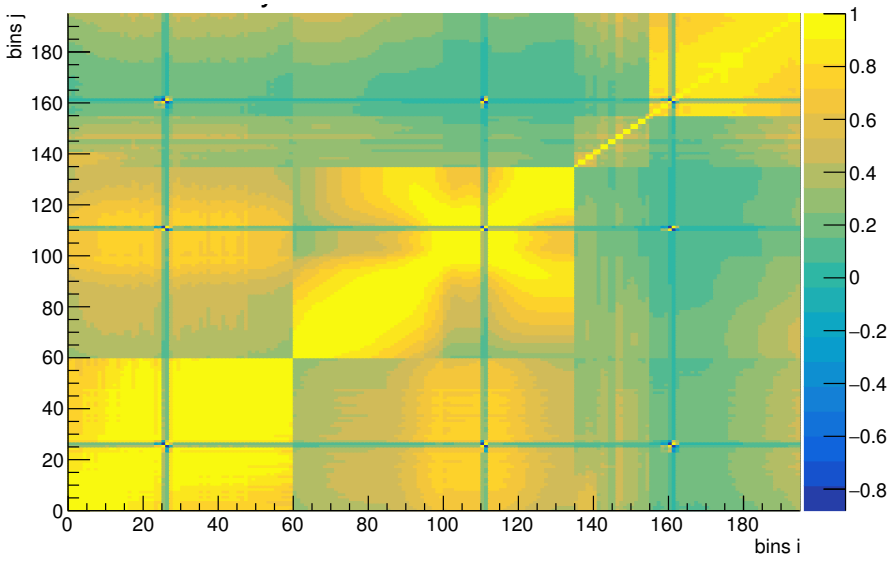

(b) Systematic correlation matrix

Figure 3. The correlation structure of the 195x195 statistical and systematic combination matrices. In each case, the axis on the right represents the overall correlation coefficient ($\rho_{ij} = -1 \leq \rho \leq 1$), where the corresponding colour indicates the degree of correlation at each point in the respective matrix (colour online).

Not doing so would result in the statistical covariance matrix having negative eigenvalues, therefore violating the condition that the covariance matrix is a positive semi-definite matrix. All remaining correlated statistical uncertainties only enter into the diagonal elements of the KLOE0812 correlation block, as they are fully correlated only for the same energy bins between the two measurements.

JHEP03(2018)173

3.2 Systematic correlations

All correlation blocks in figure 2 receive contributions from systematic uncertainties, as can be seen clearly in figure 3. Unless stated otherwise, for any two bins i and j, systematic uncertainties where correlations exist are fully correlated ($\rho_{ij} = +1$) or anti-correlated ($\rho_{ij} = -1$).

For the individual measurements, apart from two exceptions, all sources of systematic uncertainty are fully correlated between all energy bins. The first exception is the systematic uncertainty due to the unfolding, which only contributes at the sharp descent of the cross section in the $\rho - \omega$ interference region. Here, an identical unfolding uncertainty enters for five bins of the KLOE08 and KLOE12 analyses and is anti-correlated only for pairs of bins that are on different sides of this sharp descent of the cross section. For KLOE10, the only two affected bins are those directly before and directly after the sharp descent in the cross section, where the uncertainties are fully anti-correlated between these two bins. The second exception is the weighted background subtraction for KLOE12, where in the experimental analysis the weights of the fitted $e^+e^-\gamma$, $\pi\pi\gamma$ and $\pi\pi\pi$ backgrounds to the $\mu^+\mu^-\gamma(\gamma)$ spectrum are distributed over neighbouring two-bin intervals from 0.32 to 0.96 GeV^2. For the KLOE12 systematic covariance matrix, this results in only neighbouring bins from 0.36 to 0.94 GeV^2 being correlated with each other for this background subtraction uncertainty, where the first and last bin remain entirely uncorrelated in this case. A comprehensive discussion concerning this and all other systematic uncertainties for each measurement can be found in [2, 4, 6].

Importantly, for the KLOE12 systematic covariance matrix the trigger, L3 (software trigger), trackmass, tracking efficiency, acceptance and background subtraction corrections are applied to both the $\pi^+\pi^-\gamma$ and $\mu^+\mu^-\gamma$ data that enter into the ratio in equation (2.3) and, therefore, the corresponding uncertainties from a given source between the $\pi^+\pi^-\gamma$ and $\mu^+\mu^-\gamma$ data are correlated.[5] Formally, the ratio of these correction uncertainties results in a reduction of the total uncertainty of $a_\mu^{\pi^+\pi^-}$, where the contributions of the positive correlations between the KLOE08 and KLOE12 uncertainties contribute negatively to the overall uncertainty due to the partial derivative of the $\mu^+\mu^-\gamma$ data in the denominator of the ratio. However, the uncertainties due to a given source are defined in terms of the ratio of $\pi^+\pi^-\gamma$ over $\mu^+\mu^-\gamma$, such that the contributions from both data sources are already fully incorporated. Therefore, we do not separately add the uncertainties of these corrections for the $\pi^+\pi^-\gamma$ data to the KLOE12 systematic covariance matrix.

In addition, the KLOE12 systematic uncertainty vector for the non-weighted background subtraction was constructed in [5, 6] such that it contained the ratio of the contributions from the corrections of the $ee \to ee\pi\pi$ and $ee \to ee\mu\mu$ background processes, along with a trackmass (M_{trk}) tail correction, summed in quadrature. For this analysis, in order to correctly correlate these independent sources of systematic uncertainty according

[5] This only refers to the correlation of uncertainties from a specific source between the $\pi^+\pi^-\gamma$ analysis and the $\mu^+\mu^-\gamma$ analysis that enter into the KLOE12 ratio. The correlation between the KLOE08 $\pi^+\pi^-\gamma$ data and the KLOE12 cross section ratio are described in detail in the discussion of the KLOE0812 block of the systematic covariance matrix.

JHEP03(2018)173

to equation (A.5), these contributions are separated and correlated individually. This has contributed to the reduction of the KLOE12 error estimate in equation (2.7), where previously the correlation of the combined vector resulted in an incorrect overestimate of the systematic uncertainty.

For KLOE08 and KLOE10, the contributions to the systematic uncertainty from the trackmass, tracking efficiency, L3 (software trigger) efficiency, acceptance, luminosity, radiator function, vacuum polarisation correction and final state radiation correction are considered to be fully correlated in the KLOE0810 (KLOE1008) covariance matrix blocks. For the correlation of the systematic uncertainty due to the acceptance, only half of the KLOE10 uncertainty is correlated with the KLOE08 uncertainty in order to ensure that the photon detection acceptance that enters into the KLOE10 uncertainty (that is not present in the KLOE08 analyses) is not correlated and only the correlation of the pion tracks is duly accounted for. Importantly, although the KLOE08 and KLOE10 measurements only overlap for the 50 data points in the energy range 0.35 to 0.85 GeV^2, all energy bins in the 60×75 KLOE0810 (75×60 KLOE1008) correlation block must be fully correlated. Note that applying 100% correlation to only the overlapping 50×50 region would result in the systematic matrix having negative eigenvalues.

As with the statistical uncertainties for KLOE0812 (KLOE1208), the systematic uncertainties inherent in the $\pi^+\pi^-\gamma(\gamma)$ data shared between the two analyses are correlated between the KLOE08 and KLOE12 measurements. These include the uncertainties from the L3 efficiency, the background subtraction, the trackmass (M_{trk}), the unfolding, the tracking efficiency, the trigger efficiency and the acceptance from the KLOE08 analysis. The determined uncertainties for the L3, M_{trk}, tracking, trigger and acceptance corrections for KLOE12 are fully correlated for KLOE0812 such that the anti-correlation that occurs due to the ratio in KLOE12 is propagated accordingly. This is also true for the non-weighted background subtraction contribution, ensuring that only the corrections for the $ee \to ee\pi\pi$ background from the KLOE08 analysis are correlated with the ratio of the corrections of the $ee \to ee\pi\pi$ and $ee \to ee\mu\mu$ background processes as they enter in the KLOE12 analysis. The unfolding uncertainties for the KLOE0812 correlation block are, in part, anti-correlated as they are for KLOE08 and KLOE12 individually. All other systematic uncertainties are 100% correlated between KLOE08 and KLOE12.

With the same $\pi^+\pi^-\gamma(\gamma)$ data being shared between the KLOE08 and KLOE12 measurements, the KLOE1012 (KLOE1210) correlation blocks follow a similar structure to the KLOE0810 (KLOE1008) correlation blocks. The caveats to this statement are that there are no correlated uncertainties here due to the luminosity, radiator function or vacuum polarisation correction, as these effects cancel in the ratio of the $\pi^+\pi^-\gamma(\gamma)$ data over the $\mu^+\mu^-\gamma(\gamma)$ data for the KLOE12 measurement (see section 2.1). Therefore, the correlated systematic uncertainties for KLOE1012 are the trackmass, tracking efficiency, L3 efficiency, acceptance and final state radiation correction uncertainties, where it is again necessary to correlate only half of the KLOE10 acceptance uncertainty with KLOE12 in order to ensure that only the effect due to the acceptance of the pion tracks is incorporated.

JHEP03(2018)173

4 Combination and results

4.1 The combined KLOE $e^+e^- \to \pi^+\pi^-\gamma(\gamma)$ cross section

Following the methodology of section 3 yields full KLOE $\pi^+\pi^-\gamma(\gamma)$ statistical and systematic covariance matrices that describe the correlations that exist between KLOE08, KLOE10 and KLOE12. These data are combined incorporating the energy dependent statistical and systematic uncertainties and corresponding correlations, using an iterative minimisation of the following linear χ^2 function [12]

$$\chi^2 = \sum_{i=1}^{195}\sum_{j=1}^{195}\left(\sigma^0_{\pi\pi(\gamma)}(i) - \bar{\sigma}^0_{\pi\pi(\gamma)}(m)\right)\mathbf{C}^{-1}\left(i^{(m)}, j^{(n)}\right)\left(\sigma^0_{\pi\pi(\gamma)}(j) - \bar{\sigma}^0_{\pi\pi(\gamma)}(n)\right) . \tag{4.1}$$

Here, $\sigma^0_{\pi\pi(\gamma)}(i)$ is the cross section value of the data point i contributing to the combined cross section value $\bar{\sigma}^0_{\pi\pi(\gamma)}(m)$ and the combination cross section vector with the elements labelled by m contains 85 data points over the energy range $0.1 < s' < 0.95\,\mathrm{GeV}^2$, with the 85 bins corresponding to the 85 distinct energy bins of the three measurements. $\mathbf{C}^{-1}\left(i^{(m)}, j^{(n)}\right)$ is simply the inverse of the covariance matrix $\mathbf{C}\left(i^{(m)}, j^{(n)}\right)$, which is defind as the sum of the statistical covariance matrix $\mathrm{C}^{\mathrm{stat}}\left(i^{(m)}, j^{(n)}\right)$ and the systematic covariance matrix $\mathrm{C}^{\mathrm{sys}}\left(i^{(m)}, j^{(n)}\right)$. At each iterative stage of the minimisation, it is defined as

$$\mathbf{C}\left(i^{(m)}, j^{(n)}\right) = \mathrm{C}^{\mathrm{stat}}\left(i^{(m)}, j^{(n)}\right) + \frac{\mathrm{C}^{\mathrm{sys}}\left(i^{(m)}, j^{,n)}\right)}{\sigma^0_{\pi\pi(\gamma)}(i)\sigma^0_{\pi\pi(\gamma)}(j)}\bar{\sigma}^0_{\pi\pi(\gamma)}(m)\bar{\sigma}^0_{\pi\pi(\gamma)}(n)\,, \tag{4.2}$$

where the quantities $\bar{\sigma}^0_{\pi\pi(\gamma)}(m)$ and $\bar{\sigma}^0_{\pi\pi(\gamma)}(n)$ are the resulting combined cross section values from the previous iteration. This method has been adapted from [45] (see also [18]), has been advocated to be free of systematic bias and exhibits a swift convergence, after only a few iterations. We also obtain an output covariance matrix for the combined statistical and systematic uncertainties that describes the correlations between the data points of the resulting cross section vector.

The KLOE combination cross section and pion form factor data are listed in table 1. The input cross section vectors and combination covariance matrices, along with the combined output cross section vector and total covariance matrix are available from [41].[6] For the contribution to the anomalous magnetic moment of the muon in the full energy range, the KLOE combination results in

$$a_\mu^{\pi^+\pi^-}(0.10 < s' < 0.95\ \mathrm{GeV}^2) = (489.8 \pm 1.7_{\mathrm{stat}} \pm 4.8_{\mathrm{sys}}) \times 10^{-10}. \tag{4.3}$$

The resulting cross section and the individual measurements are shown in figure 4. In addition, the normalised differences of the individual KLOE measurements and the combination are shown in figure 5. We observe good agreement between the data and the combination, especially with KLOE08 which dominates the fit due to its smaller statistical uncertainty

[6] The total output matrix given contains the contributions from both the statistical and systematic uncertainties, where the choice to use both as input into the data combination results in a solution that entangles the statistical and systematic sources of uncertainty.

JHEP03(2018)173

KLOE combination					
$s'(\mathrm{GeV}^2)$	$\sigma^0_{\pi\pi(\gamma)}(\mathrm{nb})$	$\lvert F(\pi)\rvert^2$	$s'(\mathrm{GeV}^2)$	$\sigma^0_{\pi\pi(\gamma)}(\mathrm{nb})$	$\lvert F(\pi)\rvert^2$
0.105	47.27 ± 8.41	1.74 ± 0.31	0.535	1154.56 ± 6.81	35.96 ± 0.21
0.115	70.65 ± 10.44	2.04 ± 0.30	0.545	1207.69 ± 6.83	38.20 ± 0.22
0.125	80.13 ± 10.97	2.00 ± 0.27	0.555	1243.32 ± 10.13	39.94 ± 0.33
0.135	80.42 ± 11.27	1.82 ± 0.26	0.565	1285.35 ± 7.14	41.92 ± 0.23
0.145	87.58 ± 11.70	1.86 ± 0.25	0.575	1277.36 ± 7.32	42.29 ± 0.24
0.155	102.88 ± 12.35	2.10 ± 0.25	0.585	1279.89 ± 7.31	42.98 ± 0.25
0.165	115.16 ± 13.85	2.29 ± 0.28	0.595	1274.03 ± 10.32	43.27 ± 0.35
0.175	122.58 ± 13.42	2.40 ± 0.26	0.605	1228.97 ± 12.29	42.18 ± 0.42
0.185	126.19 ± 12.61	2.45 ± 0.24	0.615	950.47 ± 20.95	34.85 ± 0.77
0.195	146.34 ± 14.10	2.84 ± 0.27	0.625	803.87 ± 4.65	29.94 ± 0.17
0.205	144.18 ± 13.35	2.80 ± 0.26	0.635	781.82 ± 4.39	29.24 ± 0.16
0.215	147.47 ± 12.68	2.88 ± 0.25	0.645	731.86 ± 5.74	27.61 ± 0.22
0.225	154.64 ± 11.98	3.04 ± 0.24	0.655	679.26 ± 3.93	25.90 ± 0.15
0.235	170.47 ± 12.40	3.39 ± 0.25	0.665	620.73 ± 3.46	23.93 ± 0.13
0.245	168.96 ± 11.53	3.40 ± 0.23	0.675	569.26 ± 4.63	22.20 ± 0.18
0.255	176.55 ± 10.84	3.60 ± 0.22	0.685	518.39 ± 5.62	20.45 ± 0.22
0.265	202.38 ± 11.63	4.18 ± 0.24	0.695	471.79 ± 2.69	18.82 ± 0.11
0.275	203.28 ± 10.70	4.26 ± 0.22	0.705	431.19 ± 2.44	17.39 ± 0.10
0.285	215.28 ± 10.60	4.58 ± 0.23	0.715	386.51 ± 3.21	15.76 ± 0.13
0.295	225.63 ± 10.46	4.87 ± 0.23	0.725	356.81 ± 2.03	14.70 ± 0.08
0.305	236.90 ± 10.49	5.19 ± 0.23	0.735	327.36 ± 1.91	13.63 ± 0.08
0.315	244.65 ± 10.11	5.45 ± 0.23	0.745	299.08 ± 1.96	12.59 ± 0.08
0.325	248.45 ± 9.83	5.62 ± 0.22	0.755	273.28 ± 1.80	11.62 ± 0.08
0.335	255.64 ± 9.62	5.88 ± 0.22	0.765	249.34 ± 1.45	10.71 ± 0.06
0.345	280.05 ± 9.46	6.54 ± 0.22	0.775	228.91 ± 1.94	9.93 ± 0.08
0.355	305.24 ± 4.55	7.24 ± 0.11	0.785	211.31 ± 1.27	9.26 ± 0.06
0.365	330.21 ± 7.67	7.96 ± 0.18	0.795	196.17 ± 1.36	8.68 ± 0.06
0.375	349.58 ± 4.60	8.56 ± 0.11	0.805	183.29 ± 1.08	8.19 ± 0.05
0.385	376.70 ± 4.63	9.37 ± 0.12	0.815	170.45 ± 1.00	7.69 ± 0.05
0.395	400.82 ± 4.57	10.12 ± 0.12	0.825	157.72 ± 1.09	7.19 ± 0.05
0.405	433.99 ± 6.28	11.13 ± 0.16	0.835	146.52 ± 0.95	6.74 ± 0.04
0.415	465.70 ± 4.79	12.13 ± 0.12	0.845	136.86 ± 0.79	6.36 ± 0.04
0.425	506.53 ± 4.87	13.39 ± 0.13	0.855	126.97 ± 0.78	5.95 ± 0.04
0.435	544.42 ± 4.84	14.61 ± 0.13	0.865	119.05 ± 0.89	5.63 ± 0.04
0.445	585.65 ± 5.04	15.95 ± 0.14	0.875	111.33 ± 0.83	5.31 ± 0.04
0.455	640.09 ± 7.95	17.69 ± 0.22	0.885	104.92 ± 1.81	5.05 ± 0.09
0.465	691.86 ± 7.66	19.41 ± 0.21	0.895	98.60 ± 0.59	4.79 ± 0.03
0.475	740.82 ± 8.20	21.09 ± 0.23	0.905	93.05 ± 0.56	4.56 ± 0.03
0.485	822.23 ± 5.82	23.75 ± 0.17	0.915	87.66 ± 0.74	4.33 ± 0.04
0.495	895.61 ± 17.85	26.26 ± 0.52	0.925	82.76 ± 0.49	4.13 ± 0.02
0.505	953.15 ± 13.08	28.36 ± 0.39	0.935	78.84 ± 0.65	3.96 ± 0.03
0.515	1032.72 ± 6.28	31.20 ± 0.19	0.945	74.74 ± 0.64	3.79 ± 0.03
0.525	1078.01 ± 8.23	33.06 ± 0.25	-	-	-

Table 1. The combined KLOE measurement of the $\pi^+\pi^-\gamma(\gamma)$ bare cross section and pion form factor in $0.01\,\mathrm{GeV}^2$ intervals from $0.10 < s' < 0.95\,\mathrm{GeV}^2$. Here, s' denotes the bin centre. For both $\sigma^0_{\pi\pi(\gamma)}$ and $|F(\pi)|^2$, the error shown is the total (statistical and systematic) uncertainty. The errors have been inflated according to the local $\chi^2_{\mathrm{min}}/\mathrm{d.o.f.}$ in each energy bin, where inflation is only applied if $\chi^2_{\mathrm{min}}/\mathrm{d.o.f.} > 1$.

JHEP03(2018)173

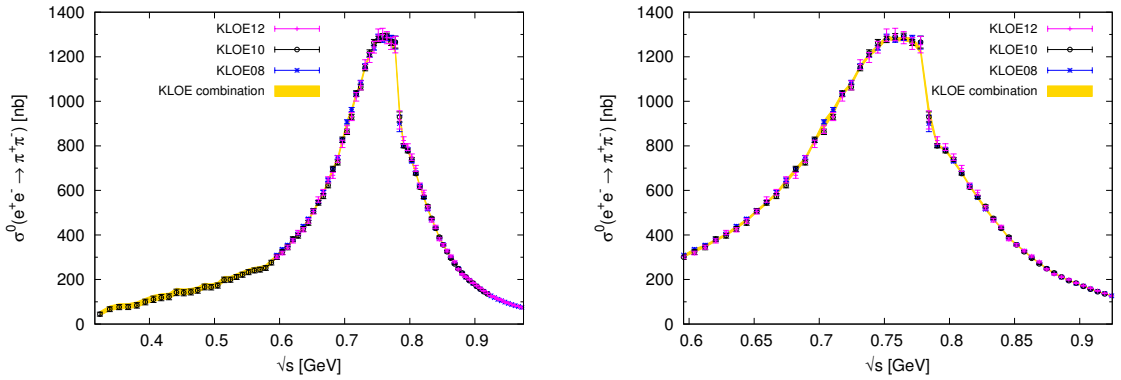

(a) Cross section in the full data range **(b)** Cross section in the overlapping data range

Figure 4. The KLOE combination plotted with the individual cross section measurements, where the KLOE combination is represented by the yellow band and the KLOE08, KLOE10 and KLOE12 cross section measurements are given by the blue, black and pink markers, respectively (colour online). In all cases, the error bars shown are the statistical and systematic uncertainties summed in quadrature.

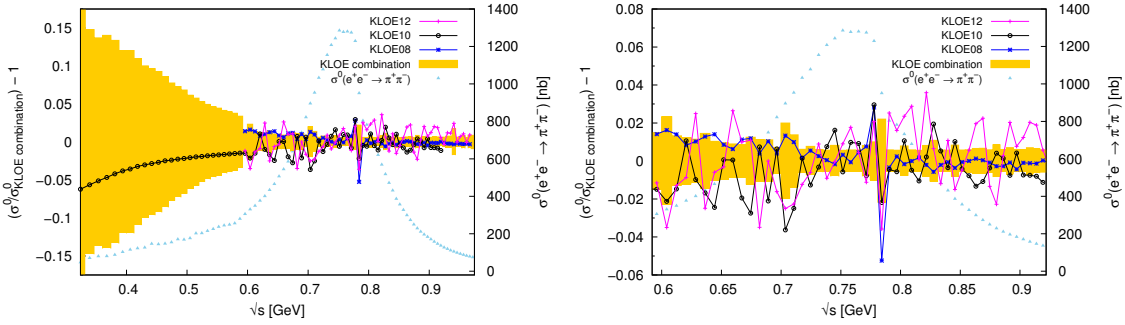

(a) Normalised difference in the full data range **(b)** Normalised difference in the overlapping data range

Figure 5. The normalised difference of the KLOE combination and the individual KLOE measurements, where the yellow band represents the statistical and systematic uncertainties of the KLOE combination summed in quadrature and the KLOE08, KLOE10 and KLOE12 cross section measurements are given by the blue, black and pink markers, respectively (colour online). Here, the errors bars of the individual measurements are not shown in order to be able to distinguish the data points, but are in good agreement with the KLOE combination.

when comparing to KLOE10 and KLOE12. KLOE12 exhibits the largest fluctuations when comparing to the fitted combination, but is well within the errors of the data. In plot (a) of figure 5, we note how the KLOE0810 and KLOE1012 systematic uncertainties have a non-trivial effect in the lower energy region where only the KLOE10 data exist, with the correlations providing an expected upward pull (which is well within the errors of the combination) to the KLOE combination cross section away from the KLOE10 data points.

JHEP03(2018)173

KLOE $\pi^+\pi^-\gamma(\gamma)$ data set	$a_\mu^{\pi^+\pi^-}(0.35 < s' < 0.85\ \mathrm{GeV}^2)$
KLOE08	$378.9 \pm 0.4_{\mathrm{stat}} \pm 3.2_{\mathrm{sys}}$
KLOE10	$376.0 \pm 0.9_{\mathrm{stat}} \pm 3.3_{\mathrm{sys}}$
KLOE12	$377.4 \pm 1.2_{\mathrm{stat}} \pm 2.3_{\mathrm{sys}}$
KLOE combination	$377.5 \pm 0.5_{\mathrm{stat}} \pm 2.1_{\mathrm{sys}}$

Table 2. Comparative results of the values obtained for $a_\mu^{\pi^+\pi^-}(0.35 < s' < 0.85\ \mathrm{GeV}^2)$ from the individual KLOE measurements and the full combination. Results for $a_\mu^{\pi^+\pi^-}$ are given in units of 10^{-10}.

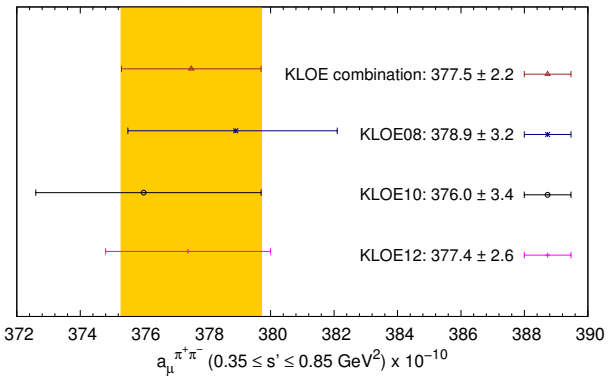

Figure 6. Comparison of estimates of $a_\mu^{\pi^+\pi^-}$ from the KLOE combination and the individual KLOE measurements in the range $0.35 < s' < 0.85\,\mathrm{GeV}^2$. The KLOE combination is represented by the yellow band (colour online). In all cases, the uncertainties shown are the statistical and systematic uncertainties summed in quadrature.

For the overlapping energy region of all three measurements, the estimates for $a_\mu^{\pi^+\pi^-}$ from the KLOE combination and the individual measurements are given in table 2 and figure 6. In all cases, the errors include all correlation contributions. For the combination, they have been inflated according to a local $\chi^2_{\mathrm{min}}/\mathrm{d.o.f.}$ in each energy bin if the $\chi^2_{\mathrm{min}}/\mathrm{d.o.f.} > 1$ [11, 46, 47], as shown in figure 7. This has resulted in an increase to the overall uncertainty of the estimate of $a_\mu^{\pi^+\pi^-}$ of $\sim 13\%$. The combination agrees well with the estimates from the individual measurements, with a marked improvement in the overall uncertainty. While the statistical uncertainty of $a_\mu^{\pi^+\pi^-}$ from the combination is dominated by KLOE08 (which has the smallest statistical uncertainty of the three individual measurements), the combination mean value of $a_\mu^{\pi^+\pi^-}$ is closest to that obtained with the KLOE12 data alone, which has the smallest systematic and, therefore, the smallest total error of the three. This in turn leads to the improved systematic error of the combined result and its markedly improved total error.

4.2 Comparison with results from the CMD-2, SND, BaBar and BESIII experiments

The $\sigma(e^+e^- \to \pi^+\pi^-)$ cross section has been measured below 1 GeV by the CMD-2 [48–50], SND [51], BaBar [52] and BESIII [53] collaborations. The BaBar and BESIII measure-

JHEP03(2018)173

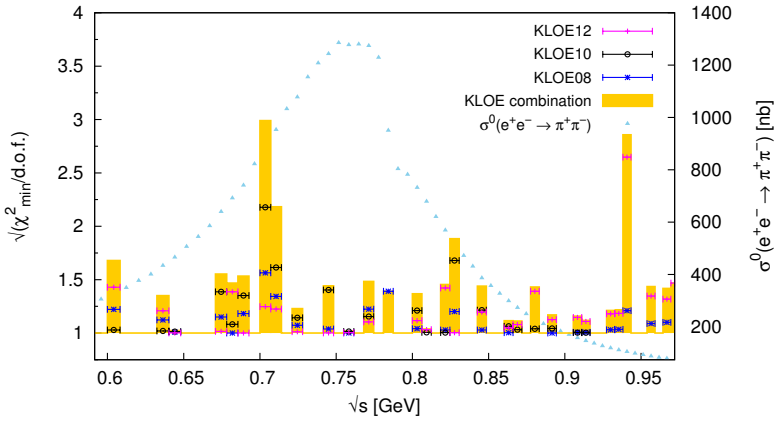

Figure 7. The effect of the local $\chi^2_{\rm min}$/d.o.f. error inflation on the KLOE combination, which is applied in each energy bin if the local $\chi^2_{\rm min}$/d.o.f. > 1. The total effect on the KLOE combination is represented by the yellow blocks (colour online). The relative contributions to each local $\chi^2_{\rm min}$/d.o.f. from the KLOE08, KLOE10 and KLOE12 measurements individually are given by the blue, black and pink markers, respectively.

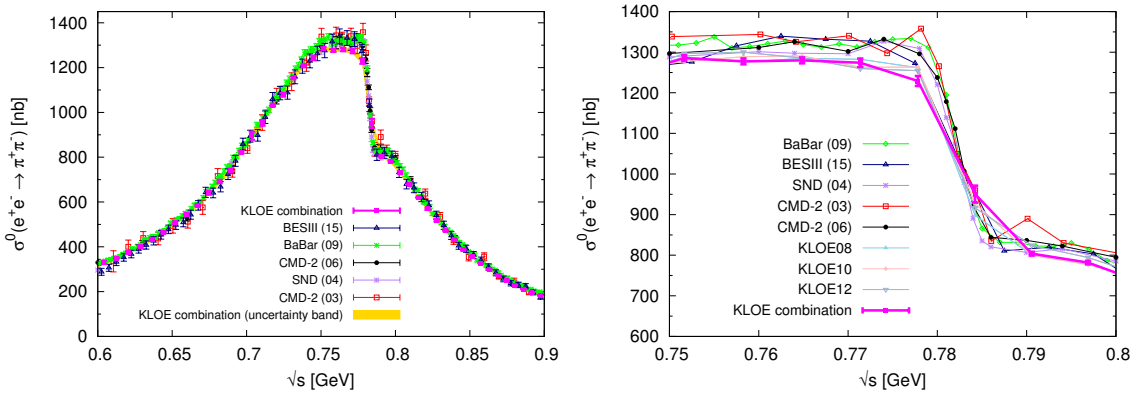

(a) Cross section in the range $0.6 < \sqrt{s'} < 0.9\,\text{GeV}$ **(b)** Cross section in the $\rho - \omega$ interference region

Figure 8. The $\pi^+\pi^-$ cross section from the KLOE combination, CMD-2 [48–50], SND [51], BaBar [52] and BESIII [53] data points. The KLOE combination is represented by the yellow band (colour online). Where uncertainties are displayed, they represent the statistical and systematic uncertainties summed in quadrature. The uncertainties of the separate experimental measurements in figure (b) have been suppressed in order to improve readability.

ments, like the KLOE measurements, are obtained through radiative return. The CMD-2 and SND measurements are taken by energy scan, allowing us to compare the two methods. All the experimental measurements are undressed of VP effects and include FSR, such that there is a consistent comparison of $\sigma^0_{\pi\pi(\gamma)}$. The cross section measurements from each experiment and the KLOE combination are shown in figure 8.

The normalised difference of the data from these experiments with respect to the KLOE combination are shown in figure 9. In particular, we note that the KLOE combination is lower than all other data at the ρ peak where the cross section is largest, but higher than

JHEP03(2018)173

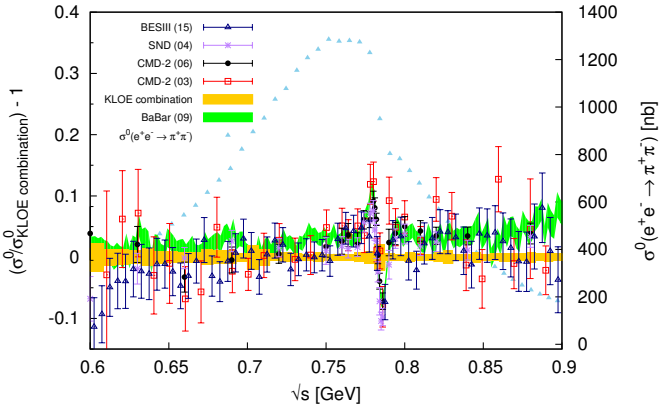

(a) KLOE combination vs. other experiments

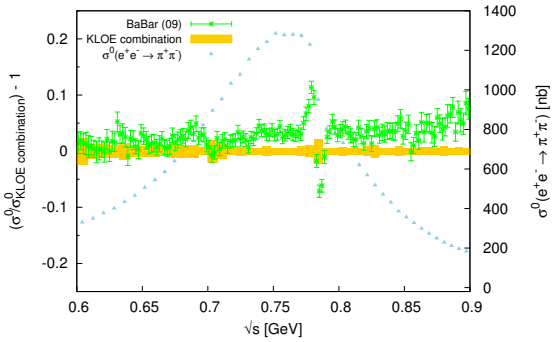

(b) KLOE combination vs. BaBar

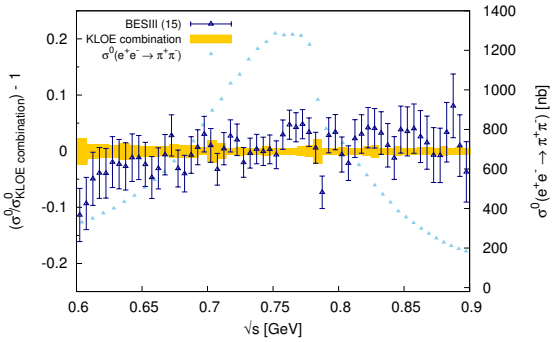

(c) KLOE combination vs. BESIII

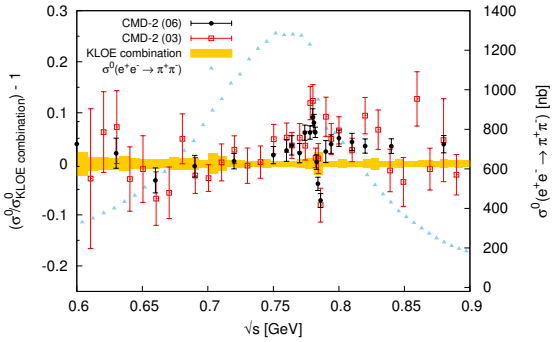

(d) KLOE combination vs. CMD-2

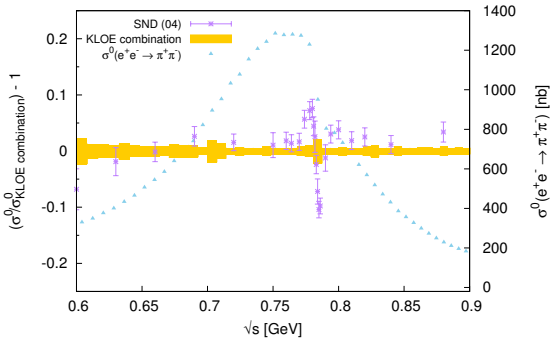

(e) KLOE combination vs. SND

Figure 9. The $\pi^+\pi^-$ cross section from the KLOE combination compared to the CMD-2, SND, BaBar and BESIII data points in the range $0.6 < \sqrt{s'} < 0.9\,\text{GeV}$. The KLOE combination is represented by the yellow band (colour online). In all cases, the uncertainties shown are the statistical and systematic uncertainties summed in quadrature.

the other experimental data where the cross section drops off in the $\rho - \omega$ interference region. This effect is evident in figure 9, where we note that for all cases (except for (c) BESIII, where the effect is less prominent), there is a sharp rise and fall of the difference in the experimental cross section at the $\rho - \omega$ interference region due to KLOE having fewer bins in this region compared to the other experiments (see plot (b) of figure 8).

JHEP03(2018)173

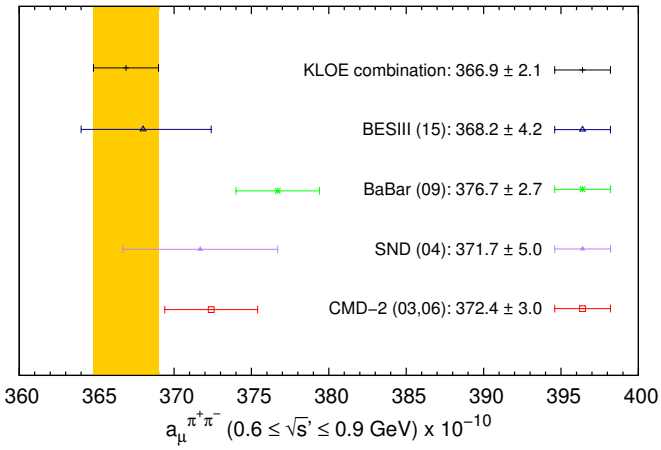

Figure 10. Estimates of $a_\mu^{\pi^+\pi^-}$ from the KLOE combination, CMD-2, SND, BaBar and BESIII in the range $0.6 < \sqrt{s'} < 0.9\,\text{GeV}$. The available CMD-2 data have been combined following the prescription of [12]. The KLOE combination is represented by the yellow band (colour online). In all cases, the uncertainties shown are the statistical and systematic uncertainties summed in quadrature.

$\pi^+\pi^-\gamma(\gamma)$ data set	$a_\mu^{\pi^+\pi^-}(0.6 < \sqrt{s'} < 0.9\ \text{GeV})$
CMD-2 fit (03,06)	372.4 ± 3.0
SND (04)	371.7 ± 5.0
BaBar (09)	376.7 ± 2.7
BESIII (15)	368.2 ± 4.2
KLOE combination	366.9 ± 2.1

Table 3. Comparative results of the values obtained for $a_\mu^{\pi^+\pi^-}(0.6 < \sqrt{s'} < 0.9\ \text{GeV})$ from the KLOE combination and the CMD-2, SND, BaBar and BESIII data. The available CMD-2 data have been combined following the prescription of [12]. Results for $a_\mu^{\pi^+\pi^-}$ are given in units of 10^{-10}. In all cases, the uncertainties shown are the statistical and systematic uncertainties summed in quadrature.

The BaBar data are, in majority, higher than the KLOE combination, whereas we observe that the other data sit mainly lower than KLOE below the ρ peak and higher above it. We also note that our comparison of the KLOE combination with the BESIII data looks markedly different from that presented in [53], especially at higher energies. However, in [53], the comparison has been made using a fit of the data to the Gounaris-Sakurai parametrisation [54], which does not provide an adequate description of the BESIII measurements of the $\pi^+\pi^-$ cross section in the tail of the resonance. We therefore opt to compare, in plot (c) of figure 9, the published BESIII data points directly with our combination of the KLOE data.

Estimates of the contribution to the anomalous magnetic moment of the muon from these experiments in the range $0.6 < \sqrt{s'} < 0.9\,\text{GeV}$ are shown in figure 10 and table 3,

JHEP03(2018)173

where we have combined the available CMD-2 data into a single estimate by applying the same method used to fit the KLOE combination. We observe good agreement (within 1.5σ) between the KLOE combination and the measurements by CMD-2, SND and BESIII. The measurement by BaBar, as evident from plot (b) of figure 9, results in a higher estimate of $a_\mu^{\pi^+\pi^-}$.

5 Conclusions

The KLOE collaboration have performed three measurements of the $\sigma^0\big(e^+e^- \to \pi^+\pi^-\gamma(\gamma)\big)$ cross section below $1\,\mathrm{GeV}^2$ using the method of radiative return. These measurements are, in part, highly correlated. This is especially true for KLOE08 and KLOE12 where, for the KLOE12 measurement, the KLOE08 $\pi^+\pi^-\gamma(\gamma)$ data is normalised by the measured $\mu^+\mu^-\gamma(\gamma)$ cross section. This has necessitated the construction of statistical and systematic combination covariance matrices, which have been carefully built to satisfy the required properties of a covariance matrix.

Using these covariance matrices, the three measurements have been combined to produce single vectors for both the two-pion cross section $\sigma_{\pi\pi(\gamma)}$ and the pion form factor $|F_\pi|^2$, along with a corresponding covariance matrix for each. This combination of the KLOE cross section data results in an estimate of the two-pion contribution to the anomalous magnetic moment of the muon of

$$a_\mu^{\pi^+\pi^-}(\text{KLOE combination}, 0.10 < s' < 0.95\ \text{GeV}^2) = (489.8 \pm 5.1) \times 10^{-10}, \qquad (5.1)$$

which is consistent with the individual KLOE measurements and within 1.5σ of the CMD-2, SND and BESIII measurements, while the difference with the BaBar data is below 3σ.

Acknowledgments

We would like to thank Fedor Ignatov for numerous useful discussions and Daisuke Nomura for his collaboration in producing the compilation and determination of the estimates of a_μ. We give special thanks to Maurice Benayoun for his studies and discussions regarding the determination of the pion form factor. We would also like to acknowledge the discussions within the *Working Group on Radiative Corrections and MC Generators for Low Energies (Radio MonteCarLOW)* [http://www.lnf.infn.it/wg/sighad/] and *The Muon* $(g-2)_\mu$ *Theory Initiative* concerning this work. The work of Alex Keshavarzi and Thomas Teubner is supported by STFC under the consolidated grants ST/N504130/1 and ST/L000431/1, respectively.

The KLOE-2 collaboration would like to warmly thank former KLOE colleagues for the access to the data collected during the KLOE data taking campaign. We thank the DAΦNE team for their efforts in maintaining low background running conditions and their collaboration during all data taking. We want to thank our technical staff: G.F. Fortugno and F. Sborzacchi for their dedication in ensuring efficient operation of the KLOE computing facilities; M. Anelli for his continuous attention to the gas system and detector safety; A. Balla, M. Gatta, G. Corradi and G. Papalino for electronics maintenance; C. Piscitelli for his help

JHEP03(2018)173

during major maintenance periods. This work was supported in part by the Polish National Science Centre through the Grants No. 2013/08/M/ST2/00323, 2013/11/B/ST2/04245, 2014/14/E/ST2/00262, 2014/12/S/ST2/00459, 2016/21/N/ST2/01727, 2016/23/N/ST2/01293.

A Properties of a covariance matrix

Any covariance matrix, $\mathcal{C}_{ij}$, of dimension $n \times n$ must satisfy the following requirements:

- As the diagonal elements of any covariance matrix are populated by the corresponding variances, all the diagonal elements of the matrix are positive. Therefore, the trace of the covariance matrix must also be positive

$$\text{Trace}(\mathcal{C}_{ij}) = \sum_{i=1}^{n} \sigma_{ii} = \sum_{i=1}^{n} \text{Var}_i > 0. \tag{A.1}$$

- It is a symmetric matrix, $\mathcal{C}_{ij} = \mathcal{C}_{ji}$, and is, therefore, equal to its transpose, $\mathcal{C}_{ij} = \mathcal{C}_{ij}^T$.

- The covariance matrix is a positive, semi-definite matrix,

$$\mathbf{a}^T \mathcal{C}\ \mathbf{a} \geq 0\ ;\ \mathbf{a} \in \mathbf{R^n}, \tag{A.2}$$

  where $\mathbf{a}$ is an eigenvector of the covariance matrix $\mathcal{C}$.

- Therefore, the corresponding eigenvalues $\lambda_{\mathbf{a}}$ of the covariance matrix must be real, greater than or equal to zero and the distinct eigenvectors are orthogonal

$$\mathbf{b}\ \mathcal{C}\ \mathbf{a} = \lambda_{\mathbf{a}}(\mathbf{b} \cdot \mathbf{a}) = \mathbf{a}\ \mathcal{C}\ \mathbf{b} = \lambda_{\mathbf{b}}(\mathbf{a} \cdot \mathbf{b}) \tag{A.3}$$

$$\therefore \text{if } \lambda_{\mathbf{a}} \neq \lambda_{\mathbf{b}} \Rightarrow (\mathbf{a} \cdot \mathbf{b}) = 0. \tag{A.4}$$

- The determinant of the covariance matrix is greater than or equal to zero: $\text{Det}(\mathcal{C}_{ij}) \geq 0$.

With error contributions from multiple sources of uncertainty for both statistics and systematics, the contributions of these individual sources must be summed correctly in order to satisfy the necessary conditions for a covariance matrix. In general, should sources of uncertainty be correlated, the element (i, j) of a covariance matrix that describes the total covariance σ_{ij} between the two data points should be constructed as

$$\mathcal{C}_{ij} \equiv \sigma_{ij} = \sum_{\alpha} \sum_{\beta} \sigma_i^{\alpha} \rho_{ij}^{\alpha\beta} \sigma_j^{\beta}\ .$$

Here, α and β denote individual sources of uncertainty, σ_i^{α} is the standard deviation of the data point i due to the uncertainty source α, σ_j^{β} is the standard deviation of the data point j due to the uncertainty source β and $\rho_{ij}^{\alpha\beta}$ is the correlation coefficient that describes the correlation $(-1 \leq \rho \leq 1)$ between the uncertainty source α of data point i and the uncertainty source β of data point j. For the construction of the KLOE covariance matrices, different sources of uncertainty are generally assumed to be independent and,

JHEP03(2018)173

therefore, uncorrelated ($\rho_{ij}^{\alpha\beta}|_{\alpha\neq\beta} = 0$). Correspondingly, we determine the element (i, j) of the covariances matrices from

$$\mathcal{C}_{ij} = \sum_{\alpha} \rho_{ij}^{\alpha} \sigma_i^{\alpha} \sigma_j^{\alpha} = \sum_{\alpha} \mathcal{C}_{ij}^{\alpha} \,, \tag{A.5}$$

where $\mathcal{C}_{ij}^{\alpha}$ is the covariance matrix specifically due to the uncertainty source α. It follows that to define the total covariance of two data points, we must know the correlation coefficient and absolute error of each data point for each source of uncertainty, which are then summed in accordance with equation (A.5).

JHEP03(2018)173

References

[1] KLOE collaboration, F. Ambrosino et al., *Measurement of $\sigma(e^+e^- \to \pi^+\pi^-\gamma(\gamma)$ and the dipion contribution to the muon anomaly with the KLOE detector*, *Phys. Lett.* **B 670** (2009) 285 [arXiv:0809.3950] [INSPIRE].

[2] S. Müller et al., *Measurement of the $\sigma(e^+e^- \to \pi^+\pi^-\gamma(\gamma))$ and the dipion contribution to the muon anomaly with the KLOE detector*, KLOE Note n. 221 (2008), http://www.lnf.infn.it/kloe/pub/knote/kn221.pdf.

[3] KLOE collaboration, F. Ambrosino et al., *Measurement of $\sigma(e^+e^- \to \pi^+\pi^-)$ from threshold to 0.85 GeV^2 using Initial State Radiation with the KLOE detector*, *Phys. Lett.* **B 700** (2011) 102 [arXiv:1006.5313] [INSPIRE].

[4] P. Beltrame et al., *Measurement of $\sigma(e^+e^- \to \pi^+\pi^-)$ for $M^2_{\pi\pi}$ between* 0.1 *and* 0.85 GeV^2 *using the Initial State Radiation method with the KLOE detector*, KLOE Note n. 225 (2011), http://www.lnf.infn.it/kloe/ppg/ppg_2010/kn225.pdf.

[5] KLOE collaboration, D. Babusci et al., *Precision measurement of $\sigma(e^+e^- \to \pi^+\pi^-\gamma)/\sigma(e^+e^- \to \mu^+\mu^-\gamma)$ and determination of the $\pi^+\pi^-$ contribution to the muon anomaly with the KLOE detector*, *Phys. Lett.* **B 720** (2013) 336 [arXiv:1212.4524] [INSPIRE].

[6] P. Lukin et al., *Precision measurement of the pion form factor $|F_\pi|^2$ from the $\pi^+\pi^-\gamma/\mu^+\mu^-\gamma$ ratio and extraction of the dipion contribution to the muon anomaly with the KLOE detector*, KLOE-2 Note K2PD-6 (2012), http://www.lnf.infn.it/kloe2/tools/getfile.php?doc_fname=K2PD-6.pdf&doc_ftype=docs.

[7] KLOE collaboration, A. Aloisio et al., *Measurement of $\sigma(e^+e^- \to \pi^+\pi^-\gamma)$ and extraction of $\sigma(e^+e^- \to \pi^+\pi^-)$ below 1-GeV with the KLOE detector*, *Phys. Lett.* **B 606** (2005) 12 [hep-ex/0407048] [INSPIRE].

[8] MUON G-2 collaboration, G.W. Bennett et al., *Measurement of the positive muon anomalous magnetic moment to 0.7 ppm*, *Phys. Rev. Lett.* **89** (2002) 101804 [*Erratum ibid.* **89** (2002) 129903] [hep-ex/0208001] [INSPIRE].

[9] MUON G-2 collaboration, G.W. Bennett et al., *Measurement of the negative muon anomalous magnetic moment to 0.7 ppm*, *Phys. Rev. Lett.* **92** (2004) 161802 [hep-ex/0401008] [INSPIRE].

[10] Muon g-2 collaboration, G.W. Bennett et al., *Final Report of the Muon E821 Anomalous Magnetic Moment Measurement at BNL*, *Phys. Rev.* **D 73** (2006) 072003 [hep-ex/0602035] [INSPIRE].

[11] Particle Data Group collaboration, C. Patrignani et al., *Review of Particle Physics*, *Chin. Phys.* **C 40** (2016) 100001 [INSPIRE].

[12] A. Keshavarzi, D. Nomura and T. Teubner, *The muon $g-2$ and $\alpha(M_Z^2)$: a new data-based analysis*, arXiv:1802.02995 [INSPIRE].

[13] K. Hagiwara, R. Liao, A.D. Martin, D. Nomura and T. Teubner, *$(g-2)_\mu$ and $\alpha(M_Z^2)$ re-evaluated using new precise data*, *J. Phys.* **G 38** (2011) 085003 [arXiv:1105.3149] [INSPIRE].

[14] M. Davier, A. Hoecker, B. Malaescu and Z. Zhang, *Reevaluation of the Hadronic Contributions to the Muon $g-2$ and to alpha(MZ)*, *Eur. Phys. J.* **C 71** (2011) 1515 [*Erratum ibid.* **C 72** (2012) 1874] [arXiv:1010.4180] [INSPIRE].

[15] M. Davier, A. Hoecker, B. Malaescu and Z. Zhang, *Reevaluation of the hadronic vacuum polarisation contributions to the Standard Model predictions of the muon $g-2$ and $\alpha(m_Z^2)$ using newest hadronic cross-section data*, *Eur. Phys. J.* **C 77** (2017) 827 [arXiv:1706.09436] [INSPIRE].

[16] F. Jegerlehner and A. Nyffeler, *The Muon $g-2$*, *Phys. Rept.* **477** (2009) 1 [arXiv:0902.3360] [INSPIRE].

[17] F. Jegerlehner, *Muon $g-2$ theory: The hadronic part*, *EPJ Web Conf.* **166** (2018) 00022 [arXiv:1705.00263] [INSPIRE].

[18] M. Benayoun, P. David, L. DelBuono and F. Jegerlehner, *Muon $g-2$ estimates: can one trust effective Lagrangians and global fits?*, *Eur. Phys. J.* **C 75** (2015) 613 [arXiv:1507.02943] [INSPIRE].

[19] B. Ananthanarayan, I. Caprini, D. Das and I. Sentitemsu Imsong, *Precise determination of the low-energy hadronic contribution to the muon $g-2$ from analyticity and unitarity: An improved analysis*, *Phys. Rev.* **D 93** (2016) 116007 [arXiv:1605.00202] [INSPIRE].

[20] Muon g-2 collaboration, J. Grange et al., *Muon $(g-2)$ Technical Design Report*, arXiv:1501.06858 [INSPIRE].

[21] J-PARC g-2 collaboration, T. Mibe, *New $g-2$ experiment at J-PARC*, *Chin. Phys.* **C 34** (2010) 745 [INSPIRE].

[22] S.J. Brodsky and E. De Rafael, *Suggested boson-lepton pair couplings and the anomalous magnetic moment of the muon*, *Phys. Rev.* **168** (1968) 1620 [INSPIRE].

[23] B.E. Lautrup and E. De Rafael, *Calculation of the sixth-order contribution from the fourth-order vacuum polarization to the difference of the anomalous magnetic moments of muon and electron*, *Phys. Rev.* **174** (1968) 1835 [INSPIRE].

[24] A. Gallo et al., *DAFNE status report*, *Conf. Proc.* **C 060626** (2006) 604 [INSPIRE].

[25] W. Kluge, *Initial state radiation: a success story*, *Nucl. Phys. Proc. Suppl.* **181-182** (2008) 280 [arXiv:0805.4708] [INSPIRE].

[26] KLOE-2 collaboration, G. Venanzoni, *From Hadronic Cross section to the measurement of the Vacuum Polarization at KLOE: a fascinating endeavour*, *EPJ Web Conf.* **166** (2018) 00021 [arXiv:1705.10365] [INSPIRE].

JHEP03(2018)173

[27] A.B. Arbuzov, E.A. Kuraev, N.P. Merenkov and L. Trentadue, *Hadronic cross-sections in electron - positron annihilation with tagged photon*, *JHEP* **12** (1998) 009 [hep-ph/9804430] [INSPIRE].

[28] M. Benayoun, S.I. Eidelman, V.N. Ivanchenko and Z.K. Silagadze, *Spectroscopy at B factories using hard photon emission*, *Mod. Phys. Lett.* **A 14** (1999) 2605 [hep-ph/9910523] [INSPIRE].

[29] S. Binner, J.H. Kuhn and K. Melnikov, *Measuring $\sigma(e^+e^- \to hadrons)$ using tagged photon*, *Phys. Lett.* **B 459** (1999) 279 [hep-ph/9902399] [INSPIRE].

[30] V.P. Druzhinin, S.I. Eidelman, S.I. Serednyakov and E.P. Solodov, *Hadron Production via e^+e^- Collisions with Initial State Radiation*, *Rev. Mod. Phys.* **83** (2011) 1545 [arXiv:1105.4975] [INSPIRE].

[31] G. Rodrigo, H. Czyz, J.H. Kuhn and M. Szopa, *Radiative return at NLO and the measurement of the hadronic cross-section in electron positron annihilation*, *Eur. Phys. J.* **C 24** (2002) 71 [hep-ph/0112184] [INSPIRE].

[32] H. Czyz, A. Grzelinska, J.H. Kuhn and G. Rodrigo, *The Radiative return at phi and B factories: Small angle photon emission at next-to-leading order*, *Eur. Phys. J.* **C 27** (2003) 563 [hep-ph/0212225] [INSPIRE].

[33] H. Czyz, A. Grzelinska, J.H. Kuhn and G. Rodrigo, *The Radiative return at Phi and B factories: FSR at next-to-leading order*, *Eur. Phys. J.* **C 33** (2004) 333 [hep-ph/0308312] [INSPIRE].

[34] H. Czyz, A. Grzelinska, J.H. Kuhn and G. Rodrigo, *The Radiative return at phi and B factories: FSR for muon pair production at next-to-leading order*, *Eur. Phys. J.* **C 39** (2005) 411 [hep-ph/0404078] [INSPIRE].

[35] Working Group on Radiative Corrections and Monte Carlo Generators for Low Energies collaboration, S. Actis et al., *Quest for precision in hadronic cross sections at low energy: Monte Carlo tools vs. experimental data*, *Eur. Phys. J.* **C 66** (2010) 585 [arXiv:0912.0749] [INSPIRE].

[36] F. Jegerlehner, *Vacuum Polarisation Correction*, (2016) www-com.physik.hu-berlin.de/~fjeger/alphaQED16.tar.gz.

[37] F. Jegerlehner, *Status and possible improvements of electroweak effective couplings for future precision experiments*, talk at *Linear Collider Workshop 2010*, http://www-com.physik.hu-berlin.de/~fjeger/SMalphas1.pdf.

[38] KLOE-2 collaboration, A. Anastasi et al., *Measurement of the running of the fine structure constant below 1 GeV with the KLOE Detector*, *Phys. Lett.* **B 767** (2017) 485 [arXiv:1609.06631] [INSPIRE].

[39] A. Hoefer, J. Gluza and F. Jegerlehner, *Pion pair production with higher order radiative corrections in low energy e^+e^- collisions*, *Eur. Phys. J.* **C 24** (2002) 51 [hep-ph/0107154] [INSPIRE].

[40] F. Jegerlehner, *Vacuum Polarisation Correction*, (2003), https://www-com.physik.hu-berlin.de/~fjeger/alphaQEDn.uu.

[41] KLOE combination $\pi^+\pi^-\gamma$ (ppg) data web link (2017), http://www.lnf.infn.it/kloe/ppg/ppg_2017/ppg_2017.html.

JHEP03(2018)173

[42] S. Müller, *The Why's and How's of covariance matrices in the KLOE ISR analyses*, in *Constraining the Hadronic Contributions to the Muon Anomalous Magnetic Moment*, arXiv:1306.2045 [INSPIRE].

[43] G. D'Agostini, *A Multidimensional unfolding method based on Bayes' theorem*, *Nucl. Instrum. Meth.* **A 362** (1995) 487 [INSPIRE].

[44] G. D'Agostini, *Improved iterative Bayesian unfolding*, arXiv:1010.0632.

[45] NNPDF collaboration, R.D. Ball et al., *Fitting Parton Distribution Data with Multiplicative Normalization Uncertainties*, *JHEP* **05** (2010) 075 [arXiv:0912.2276] [INSPIRE].

[46] S. Eidelman and F. Jegerlehner, *Hadronic contributions to $g-2$ of the leptons and to the effective fine structure constant $\alpha(M_z^2)$*, *Z. Phys.* **C 67** (1995) 585 [hep-ph/9502298] [INSPIRE].

[47] M. Davier, A. Hoecker, B. Malaescu, C.Z. Yuan and Z. Zhang, *Reevaluation of the hadronic contribution to the muon magnetic anomaly using new $e^+e^- \to \pi^+\pi^-$ cross section data from BABAR*, *Eur. Phys. J.* **C 66** (2010) 1 [arXiv:0908.4300] [INSPIRE].

[48] R.R. Akhmetshin et al., *Measurement of the $e^+e^- \to \pi^+\pi^-$ cross section with the CMD-2 detector in the 370–520 MeV c.m. energy range*, *JETP Lett.* **84** (2006) 413 [hep-ex/0610016] [INSPIRE].

[49] CMD-2 collaboration, R.R. Akhmetshin et al., *High-statistics measurement of the pion form factor in the rho-meson energy range with the CMD-2 detector*, *Phys. Lett.* **B 648** (2007) 28 [hep-ex/0610021] [INSPIRE].

[50] CMD-2 collaboration, R.R. Akhmetshin et al., *Reanalysis of hadronic cross-section measurements at CMD-2*, *Phys. Lett.* **B 578** (2004) 285 [hep-ex/0308008] [INSPIRE].

[51] M.N. Achasov et al., *Update of the $e^+e^- \to \pi^+\pi^-$ cross-section measured by SND detector in the energy region $400 < \sqrt{s} < 1000$ MeV*, *J. Exp. Theor. Phys.* **103** (2006) 380 [hep-ex/0605013] [INSPIRE].

[52] BABAR collaboration, B. Aubert et al., *Precise measurement of the $e^+e^- \to \pi^+\pi^-(\gamma)$ cross section with the Initial State Radiation method at BABAR*, *Phys. Rev. Lett.* **103** (2009) 231801 [arXiv:0908.3589] [INSPIRE].

[53] BESIII collaboration, M. Ablikim et al., *Measurement of the $e^+e^- \to \pi^+\pi^-$ cross section between 600 and 900 MeV using initial state radiation*, *Phys. Lett.* **B 753** (2016) 629 [arXiv:1507.08188] [INSPIRE].

[54] G.J. Gounaris and J.J. Sakurai, *Finite width corrections to the vector meson dominance prediction for $\rho \to e^+e^-$*, *Phys. Rev. Lett.* **21** (1968) 244 [INSPIRE].

JHEP03(2018)173